Supplemental Information

for

Structural basis for enhanced neutralization of HIV-1 by a dimeric IgG form of the glycan-recognizing antibody 2G12

Yunji Wu[1], Anthony P. West, Jr.[1], Helen J. Kim[2], Matthew E. Thornton[1,3], Andrew B. Ward[2], Pamela J. Bjorkman[1,4,*]

[1]Division of Biology and Biological Engineering 114-96, California Institute of Technology, 1200 East California Boulevard, Pasadena, CA 91125, USA

[2]Department of Integrative Structural and Computational Biology, The Scripps Research Institute, La Jolla, CA 92037, USA

[3]Present address: University of Southern California Keck School of Medicine, Division of Maternal Fetal Medicine at the Saban Research Institute of Children's Hospital of Los Angeles, Los Angeles, CA 90027, USA

[4]Howard Hughes Medical Institute, California Institute of Technology, 1200 East California Boulevard, Pasadena, CA 91125, USA

*Correspondence should be addressed to: bjorkman@caltech.edu

Supplemental Results

Calculation of interchain distances for connectivity model for 2G12 dimer/2G12.1 peptide complex

Nineteen residues within the 2G12 hinge region were missing from the $(Fab)_2$ (pdb ID 1OP3) and Fc (pdb ID 1H3X) structures used as search models for molecular replacement. Distances from the N-termini of the four Fc polypeptide chains to the C-termini of the four $(Fab)_2$ heavy chains were measured using coordinates for high resolution models placed into the 2G12 dimer/2G12.1 structure for residues Pro-238 (N-terminus of Fc) and Lys-228 (C-terminus of the $(Fab)_2$ heavy chain) (residue numbering based on the structures of 2G12 $(Fab)_2$ (pdb ID 1OP3) and Fc (pdb ID 1H3X)).

Solution studies of 2G12 monomer and 2G12 dimer

Small-angle X-ray scattering (SAXS) can be used to derive *ab initio* information about the size, shape and flexibility of proteins in solution (Putnam et al., 2007). To obtain independent structural information for 2G12 dimer, we used SAXS to investigate the conformational range of 2G12 dimer (Figure S5). We obtained X-ray scattering profiles (Figure S5E) from solutions of purified 2G12 monomer, 2G12 dimer, and Rituximab, a conventional monomeric human IgG (Anderson et al., 1997). For each protein, we generated 10 *ab initio* models (Figure S5A-C) using DAMMIF (Franke, 2009), which were superposed, averaged, and filtered using DAMAVER (Volkov, 2003). Models filled with dummy atoms showed 2G12 monomer as a relatively rigid “slab” with potential flexibility only at the hinge region between the $(Fab)_2$ unit and the Fc (Figure S5A). In contrast, models of 2G12 dimer showed a larger molecule with

increased conformational flexibility (Figure S5B). Rituximab models showed a thinner but conformationally similar molecule to 2G12 dimer (Figure S5C).

The distance distribution function *P(r)* was derived through an indirect Fourier transform of the scattering curve using GNOM (Svergun, 1992). *P(r)* was monomodal for 2G12 monomer and 2G12 dimer (Figure S5D), corresponding to the profile for a globular protein. *P(r)* for Rituximab exhibited a smaller second peak, suggesting the presence of more elongated domains in solution (Figure S5D) (Putnam et al., 2007). *P(r)* functions for all three proteins converged smoothly to zero at D_{max}, which corresponded to the maximum linear dimension of the scattering particles: 162 Å for 2G12 monomer, 178 Å for Rituximab, and 193 Å for 2G12 dimer. The differences in apparent size in solution corroborated our findings from the crystal structures of 2G12 dimer – as predicted, the gyration space that 2G12 dimer occupied in solution was larger than that of both 2G12 monomer and Rituximab. 2G12 monomer, which should exhibit limited mobility due to the $(Fab)_2$ domain exchange, indeed had a lower R_g than both conventional IgG and 2G12 dimer (Guinier analysis yielded R_g values of 46 ± 0.42 Å, 52 ± 2.3 Å, and 59 ± 0.67 Å, for 2G12 monomer, Rituximab, and 2G12 dimer, respectively, see Figure S5D). Rituximab also exhibited a broader R_g distribution in Guinier analysis than both 2G12 monomer and dimer, suggesting that the conventional IgG was more flexible in solution than 2G12 dimer. 2G12 dimer was in turn more flexible than 2G12 monomer, which exhibited the narrowest R_g distribution. The reference model chosen by DAMAVER produced a .fir file in DAMMIF, which was used to calculate a back-transform of the final averaged models (Figure S5E). Simulated scattering from the averaged models fit the experimental scattering data well, with χ^2 of fit values between I_{exp} and I_{sim} of 1.347, 1.202, and 1.218 for 2G12 monomer, 2G12 dimer, and control IgG Rituximab, respectively (Figure S5E).

Supplemental Experimental Procedures

Protein expression and purification

Purified monomeric HIV-1 gp120 was a gift from Leo Stamatatos and Zachary Caldwell (Seattle BioMed) (Sharma et al., 2006). Purified 2G12 $(Fab)_2$ was a gift from Zara Fulton and was imaged by Reza Khayat (The Scripps Research Institute). Other reagents, such as control monomeric IgGs and purified soluble rat FcRn (which binds human IgG equally as well as rat IgG (Huber, 1994)) were provided by members of the Bjorkman laboratory including Paola Marcovecchio, Han Gao, Maria Politzer, and Kathryn Huey Tubman. Protein concentrations were determined spectrophotometrically using extinction coefficients at 280 nm of 200480 M^{-1} cm^{-1} (2G12 monomer), 400960 M^{-1} cm^{-1} (2G12 dimer), 202000 M^{-1} cm^{-1} (conventional monomeric IgG antibodies), 84900 M^{-1} cm^{-1} (rat FcRn), and 146090 M^{-1} cm^{-1} (SF162 gp120). Extinction coefficients were calculated based on amino acid compositions using ProtParam (Artimo et al., 2012).

Crystallization and data collection

Crystals of 2G12 dimer (space group $P6_122$) were grown in hanging drops by mixing equal volumes of 2G12 dimer (11.5 mg/ml) with a solution containing 1.2 M ammonium sulfate, and 100 mM HEPES pH 7.0 at 20º C. Crystals were cryopreserved in well solution containing 25-30% glycerol. Data were collected to 7.5 Å resolution at beamline 8.3.1 of the Advanced Light Source (ALS) at Lawrence Berkeley National Laboratory (LBNL), and at beamline 12-2 of the Stanford Synchrotron Radiation Lightsource (SSRL) at the SLAC National Accelerator Laboratory. Over 500 crystals were screened, but all diffracted poorly and were fragile to handle. Experiments to improve the quality of the crystals included seeding, glutaraldehyde

crosslinking, recrystallization, additives, exchanging into lithium sulfate, exploring cryoprotectants, and varying drop composition. Tantalum bromide clusters (Jena Biosciences) were soaked into the native crystals, resulting in bright green crystals. SAD data with reflections to 10 Å were collected at beamline 8.3.1 of the ALS at LBNL at a single wavelength of 1.255 Å.

For crystallization of the 2G12 dimer/2G12.1 complex, 2G12.1 peptide (The Polypeptide Group) was mixed with 2G12 dimer (11.5 mg/ml) at a 19:1 molar ratio in 24-well hanging drops of protein and reservoir solution in equal amounts. Clustered hexagonal crystals formed from spherolites by vapor diffusion in 5% Tascimate, 10% PEGMME 5000, and 100 mM HEPES at pH 7.0. Crystals were cryopreserved in the well solution containing 30% PEGMME 5000 and screened at beamline BL12-2 at the SSRL at SLAC, and the 5 μm microbeam at beamline 23ID-D at the General Medical Sciences and Cancer Institutes Structural Biology Facility (GM/CAT) at the Advanced Photon Source (APS). Upon handling, the clustered crystals occasionally disintegrated into smaller, more singular pieces, which were also cryoprotected and screened. We also collected usable data sets from large crystals (0.3 mm diameter) that contained singular patches.

Model validation calculations

Calculations using derivative crystals were performed using software in the CCP4 Software Suite (Winn et al., 2011) via the ccp4i graphical user interface (Potterton et al., 2003): cad (Winn et al., 2011), scaleit (Winn et al., 2011), fft (Read, 1988), followed by Phenix.autosol (Adams et al., 2010), and Phenix.emma (Adams et al., 2010).

Small angle X-ray scattering (SAXS)

Samples for SAXS were concentrated to 17 mg/ml (2G12 monomer), 13 mg/ml (2G12 dimer), and 21 mg/ml (Rituximab) and filtered through 0.22 μm membranes. Dialysis to buffer exchange

each protein into Phosphate Buffered Saline was performed overnight, and samples were diluted for a concentration series of 0.25 mg/ml, 0.5 mg/ml, 0.75 mg/ml, 1.0 mg/ml, 2.5 mg/ml, 5.0 mg/ml, and 7.5 mg/ml, along with 1-3% glycerol to minimize aggregation caused by radiation damage. Data were collected at SSRL beamline 4-2 using a Rayonix MX225-HE detector at a distance of 2500 mm, using 1.13 Å wavelength X-rays. For each concentration of each sample, 15 exposures of 1 second were collected, covering a momentum transfer (q) range of 0.0047–0.375 1/Å. The scattering profile for the buffer was obtained in the same manner and subtracted from the protein profiles. The detector images were integrated, background subtracted, and screened for radiation damage using SasTool (Smolsky, 2007). Extrapolation to infinite dilution was done with PRIMUS (Konarev, 2003). Guinier analysis was performed using AutoRG, distance distribution functions determined with GNOM (Svergun, 1992), and *ab initio* reconstructions were performed using DAMMIF (Franke, 2009) and DAMAVER (Volkov, 2003) in the ATSAS package (Petoukhov et al., 2012).

Supplemental Table

Table S1. Data Collection and Refinement Statistics

	2G12 dimer	2G12 dimer with $(Ta_6Br_{12})^{2+}$	2G12/2G12.1 peptide
Data Collection			
Resolution (Å)	39.8-8.0 (8.3-8.0)	35.0-10.0 (10.34-10.0)	64.9-6.5 (6.7-6.5)
Space group	$P6_12\ 2$	$P6_12\ 2$	P6
Unit cell	*a* = *b* = 246 Å *c* = 657 Å α = β = 90° γ = 120°	*a* = *b* = 250 Å *c* = 652 Å α = β = 90° γ = 120°	*a* = *b* = 375 Å *c* = 64 Å α = β = 90° γ = 120°
Total reflections	26016 (2520)	90570	113124 (11045)
Unique reflections	12654 (1260)	11087 (483)	10665 (1022)
Completeness (%)	96.95 (71.03)	99.0 (89.6)	99.96 (100.00)
Mean I/σ(I)	6.51 (1.72)	7.6 (1.3)	7.84 (1.51)
R_{merge}	0.088 (0.46)	0.33 (0.78)	0.28 (2.1)
CC½	0.99 (0.80)		1.0 (0.83)
CC*	1.0 (0.94)		1.0 (0.95)
R_{anom}		0.22 (0.87)	
Anomalous completeness		74.6 (74.4)	
Anomalous multipicity		4.6 (4.7)	
f'		-26.4	
f''		17.0	
Refinement			
R_{work}	0.35 (0.35)		0.38 (0.44)
R_{free}	0.37 (0.36)		0.36 (0.39)
Number of atoms	29250		28984
Protein residues	3795		3750
RMS bonds (Å)	0.018		0.037
RMS angles (°)	1.62		1.78
Average B-factor (Å^2)	159.0		481.0

*Statistics for the highest-resolution shell are shown in parentheses.

Supplemental Figure Legends

Figure S1. Proposed connectivities of 2G12 dimer and 2G12 trimer, related to Figure 1

(A,B) Schematic diagrams illustrating how intermolecular domain swapping could lead to 2G12 dimer (A) and 2G12 trimer (B). The connectivity model allows for the formation of higher order multimers, including tetramers (panel C). (C) Size exclusion chromatography profile for 2G12 proteins after elution from an FcRn affinity column. Peaks labeled as monomer and dimer were identified using in-line static light scattering to determine their molecular masses (West et al., 2009). Peaks migrating at higher apparent molecular weights are labeled as trimer and tetramer.

Figure S2. Heavy atom validation of molecular replacement phases, related to Figure 2

Data were collected from crystals of 2G12 dimer soaked with tantalum bromide clusters to 10 Å resolution at a wavelength of 1.255 Å, chosen to maximize the anomalous diffraction signal of tantalum. Using phases derived from the molecular replacement model, we calculated both anomalous and isomorphous difference Fourier maps, which each yielded a set of peaks, seven of which were common to both maps. We checked the top five potential heavy atom sites by iteratively omitting one site, calculating phases with the remaining sites, and then examining difference Fourier maps to see if the omitted site was found. Two of the five potential sites, iteratively omitted in this way, were independently reproduced. In each calculation of an isomorphous difference Fourier map during cross-phasing, three additional sites were consistently and independently produced. One site was reproduced in the calculations of anomalous difference Fourier maps during cross-phasing. We concluded that the three sites that survived the cross-phasing process after appearing consistently in both isomorphous and anomalous difference Fourier maps corresponded to tantalum bromide clusters. The putative

tantalum bromide sites corresponded to locations on the surface of the 2G12 dimer model. (A) Heavy atom sites (colored spheres) on dimer B/C from Figure 2. (B) Heavy atom sites on dimer A from Figure 2.

Figure S3. Packing of 2G12/2G12.1 peptide crystals, related to Figure 3

Half of a unit cell containing three copies of the asymmetric unit in space group P6 is shown. The asymmetric unit contains one intact 2G12 dimer (two $(Fab)_2$ units and two Fcs; yellow Cα trace) and half of a second 2G12 dimer (one $(Fab)_2$ unit and one Fc; magenta Cα trace). Rotation around a crystallographic two-fold axis creates the second half of the magenta dimer, which is conformationally the same as the yellow dimer. (A) Green circles show locations of antigen binding sites, which do not contact each other in the P6 crystals. Addition of 2G12.1 peptide to 2G12 dimer disrupted the crystal contacts at the antigen binding sites in the $P6_122$ 2G12 dimer crystals (Figure 2A). (B) Blue circles highlight crystal contacts between Fc regions. Similar crystal contacts were found in the $P6_122$ 2G12 dimer crystals (Figures 2C, 3C). (C) 2G12/2G12.1 structure shown as a volume representation (Figure 4C) superimposed on the locations of the yellow dimers (left) and magenta dimers (right).

Figure S4. Distinct 2G12 dimer structures, related to Figure 4

Dimer structures are shown as 25 Å electron density envelopes calculated from $(Fab)_2$ and Fc coordinates located by molecular replacement calculations. Side indicates dimers shown with side views of $(Fab)_2$ units, top indicates a view in which Fc regions point into the page, and bottom indicates a view in which Fc regions point out of the page. (A) Dimer A from Figure 2 (cyan) (Figure 4A). (B) Dimers B and C from Figure 2 (magenta and indigo) (Figure 4B). (C) Dimer from 2G12/2G12.1 peptide structure (Figure 4C).

The symmetry of two of the 2G12 dimer conformations, dimer A and the dimer in the 2G12/2G12.1 peptide structure (panels A and C), was point group C2 (the dimer two-fold symmetry axis was coincident with a crystallographic two-fold axis). The dimer B/C conformation (panel B) represented a distortion from C2 symmetry. A 2G12 dimer could also have point group D2 symmetry with the $(Fab)_2$ units in a similar position as in a C2 dimer except with their internal two-fold axes coincident, and with the Fcs above and below the plane of the $(Fab)_2$ units with the Fc two-fold axes coincident with each other and perpendicular to the $(Fab)_2$ two-fold axes. Although the D2 conformation appeared plausible, it was not observed in our structures. To interconvert these forms would require one $(Fab)_2$ unit to rotate 180˚.

Figure S5. SAXS Data for 2G12 monomer, dimer, and a conventional IgG monomer, related to Figure 5

Ab initio models filled with dummy atoms revealing size and shape of (A) 2G12 monomer, (B) 2G12 dimer, and (C) Rituximab, a conventional IgG monomer. (D) Pair-distribution functions and Guinier plots from 2G12 monomer, dimer, and Rituximab. Guinier plots calculated from low *q* ranges behaved linearly, indicating minimal aggregation (Hammel, 2012; Mertens and Svergun, 2010). Differences in D_{max} calculated from *P(r)* were consistent with 2G12 monomer's comparatively smaller range of motion and Rituximab's more freely mobile domains compared to 2G12 dimer. (E) Data analyses. Left: Scattering profiles of 2G12 monomer, 2G12 dimer, and Rituximab, plotted as log(I) vs. *q*. Profiles from all concentrations of each protein were superimposable when scaled by concentration, indicating low inter-particle forces, properly folded species, and ideal sample quality. Accordingly, one representative scattering profile was chosen from the concentration series for each individual protein, and merging of multiple scattering profiles was not required. Second from left: Traditional Kratky analysis used for detecting conformational flexibility via visual inspection (Putnam et al., 2007). Bimodal profiles

for 2G12 dimer and Rituximab revealed behavior similar to that of a heterogeneous mixture of species. 2G12 dimer exhibited a slowly increasing curve at large *q* values, suggesting an elongated species when compared to Rituximab and 2G12 monomer. Third from left: Analysis of samples using Porod-Debye law revealed a loss of plateau in Rituximab when compared with 2G12 monomer, indicating increased flexibility. 2G12 dimer exhibited a divergent curve at large *q* values, characteristic of an elongated species (Hammel, 2012). Right: Simulated scattering from DAMAVER averaged models (red, green, or blue) fit to the experimental scattering data (gray), plotted as log(I) vs. *q*.

Figure S6. SPR sensorgrams containing residuals of 1:1 binding model fits, related to Figure 6

Sensorgrams were derived from binding experiments in which 2G12 monomer, 2G12 dimer, or a conventional monomeric anti-gp120 IgG was injected over immobilized gp120 from HIV-1 strain SF162. Experimental data (colored lines) were fit to a 1:1 binding model (black lines). Residual plots are shown in Figure S6. (A) 2G12 monomer, 2G12 dimer, and a conventional anti-gp120 IgG (NIH45-46^{G54W}) injected over gp120 immobilized at high coupling density (~100 RU). 2G12 monomer, but not 2G12 dimer or the conventional IgG, could be fit to a 1:1 binding model. (B) 2G12 monomer, 2G12 dimer, and a conventional anti-gp120 IgG (NIH45-46^{G54W}) injected over gp120 immobilized at medium coupling density (~50 RU). 2G12 monomer, but not 2G12 dimer or the conventional IgG, could be fit to a 1:1 binding model. (C) 2G12 monomer, 2G12 dimer, and a conventional anti-gp120 IgG (2909) injected over gp120 immobilized at low coupling density (<10 RU). All could be fit to a 1:1 binding model.

Supplemental References

Adams, P.D., Afonine, P.V., Bunkoczi, G., Chen, V.B., Davis, I.W., Echols, N., Headd, J.J., Hung, L.W., Kapral, G.J., Grosse-Kunstleve, R.W.*, et al.* (2010). PHENIX: a comprehensive Python-based system for macromolecular structure solution. Acta crystallographica Section D, Biological crystallography *66*, 213-221.

Anderson, D.R., Grillo-Lopez, A., Varns, C., Chambers, K.S., and Hanna, N. (1997). Targeted anti-cancer therapy using rituximab, a chimaeric anti-CD20 antibody (IDEC-C2B8) in the treatment of non-Hodgkin's B-cell lymphoma. Biochemical Society transactions *25*, 705-708.

Artimo, P., Jonnalagedda, M., Arnold, K., Baratin, D., Csardi, G., de Castro, E., Duvaud, S., Flegel, V., Fortier, A., Gasteiger, E.*, et al.* (2012). ExPASy: SIB bioinformatics resource portal. Nucleic acids research *40*, W597-603.

Burmeister, W.P., Huber, A.H., and Bjorkman, P.J. (1994). Crystal structure of the complex of rat neonatal Fc receptor with Fc. Nature *372*, 379-383.

Franke, D.S., D. I. (2009). DAMMIF, a program for rapid ab-initio shape determination in small-angle scattering. J Appl Cryst *42*, 342-346.

Hammel, M. (2012). Validation of macromolecular flexibility in solution by small-angle X-ray scattering (SAXS). European biophysics journal : EBJ *41*, 789-799.

Huber, A.H. (1994). Biochemical and Structural Characterization of Drosophila Neuroglian. In Division of Biology (Pasadena, CA: California Institute of Technology).

Huber, A.H., Kelley, R.F., Gastinel, L.N., and Bjorkman, P.J. (1993). Crystallization and stoichiometry of binding of a complex between a rat intestinal Fc receptor and Fc. Journal of molecular biology *230*, 1077-1083.

Hummel, J.P., and Dreyer, W.J. (1962). Measurement of protein-binding phenomena by gel filtration. Biochimica et biophysica acta *63*, 530-532.

Konarev, P.V., Volkov, V. V, Sokolava, A. V., Koch, M. H. J., and Svergun, D. I. (2003). PRIMUS - a Windows-PC based system for small-angle scattering data analysis. . J Appl Cryst *36*, 1277-1282.

Mertens, H.D., and Svergun, D.I. (2010). Structural characterization of proteins and complexes using small-angle X-ray solution scattering. Journal of structural biology *172*, 128-141.

Petoukhov, M.V., Franke, D., Shkumatov, A.V., Tria, G., Kikhney, A.G., Gajda, M., Gorba, C., Mertens, H.D.T., Konarev, P.V., and Svergun, D.I. (2012). New developments in the ATSAS program package for small-angle scattering data analysis. Journal of applied crystallography *45*, 342-350.

Potterton, E., Briggs, P., Turkenburg, M., and Dodson, E. (2003). A graphical user interface to the CCP4 program suite. Acta crystallographica Section D, Biological crystallography *59*, 1131-1137.

Putnam, C.D., Hammel, M., Hura, G.L., and Tainer, J.A. (2007). X-ray solution scattering (SAXS) combined with crystallography and computation: defining accurate macromolecular structures, conformations and assemblies in solution. Quarterly reviews of biophysics *40*, 191-285.

Read, R.J.S., A. J. (1988). A phased translation function. J Appl Cryst *21*, 490-495.

Sanchez, L.M., Penny, D.M., and Bjorkman, P.J. (1999). Stoichiometry of the interaction between the major histocompatibility complex-related Fc receptor and its Fc ligand. Biochemistry *38*, 9471-9476.

Sharma, V.A., Kan, E., Sun, Y., Lian, Y., Cisto, J., Frasca, V., Hilt, S., Stamatatos, L., Donnelly, J.J., Ulmer, J.B.*, et al.* (2006). Structural characteristics correlate with immune responses induced by HIV envelope glycoprotein vaccines. Virology *352*, 131-144.

Smolsky, I., Liu, P., Niebuhr, M., Ito, K., Weiss, T. M., Tsuruta, H. (2007). Biological small-angle X-ray scattering facility at the Stanford Synchrotron Radiation Laboratory. J Appl Cryst *40*, 453-458.

Svergun, D.I. (1992). Determination of the regularization parameter in indirect-transform methods using perceptual criteria J Appl Cryst *25*, 495-503.
Volkov, V.S., D. (2003). Uniqueness of ab-initio shape determination in small-angle scattering. J Appl Cryst *36*, 860-864.
West, A.P., Jr., and Bjorkman, P.J. (2000). Crystal structure and immunoglobulin G binding properties of the human major histocompatibility complex-related Fc receptor(,). Biochemistry *39*, 9698-9708.
West, A.P., Jr., Galimidi, R.P., Foglesong, C.P., Gnanapragasam, P.N., Huey-Tubman, K.E., Klein, J.S., Suzuki, M.D., Tiangco, N.E., Vielmetter, J., and Bjorkman, P.J. (2009). Design and expression of a dimeric form of human immunodeficiency virus type 1 antibody 2G12 with increased neutralization potency. Journal of virology *83*, 98-104.
Winn, M.D., Ballard, C.C., Cowtan, K.D., Dodson, E.J., Emsley, P., Evans, P.R., Keegan, R.M., Krissinel, E.B., Leslie, A.G., McCoy, A.*, et al.* (2011). Overview of the CCP4 suite and current developments. Acta crystallographica Section D, Biological crystallography *67*, 235-242.

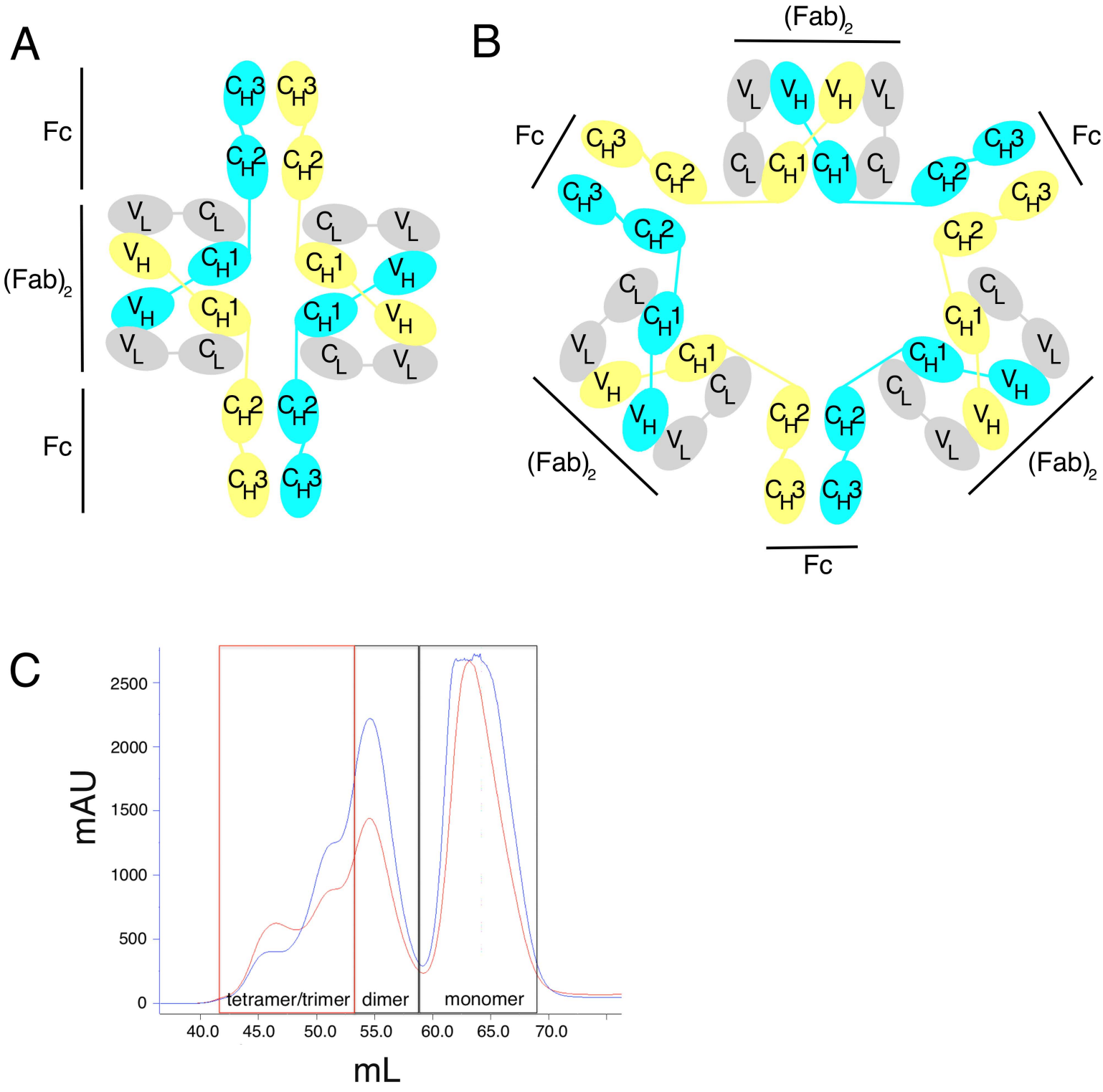

Figure S1, related to Figure 1

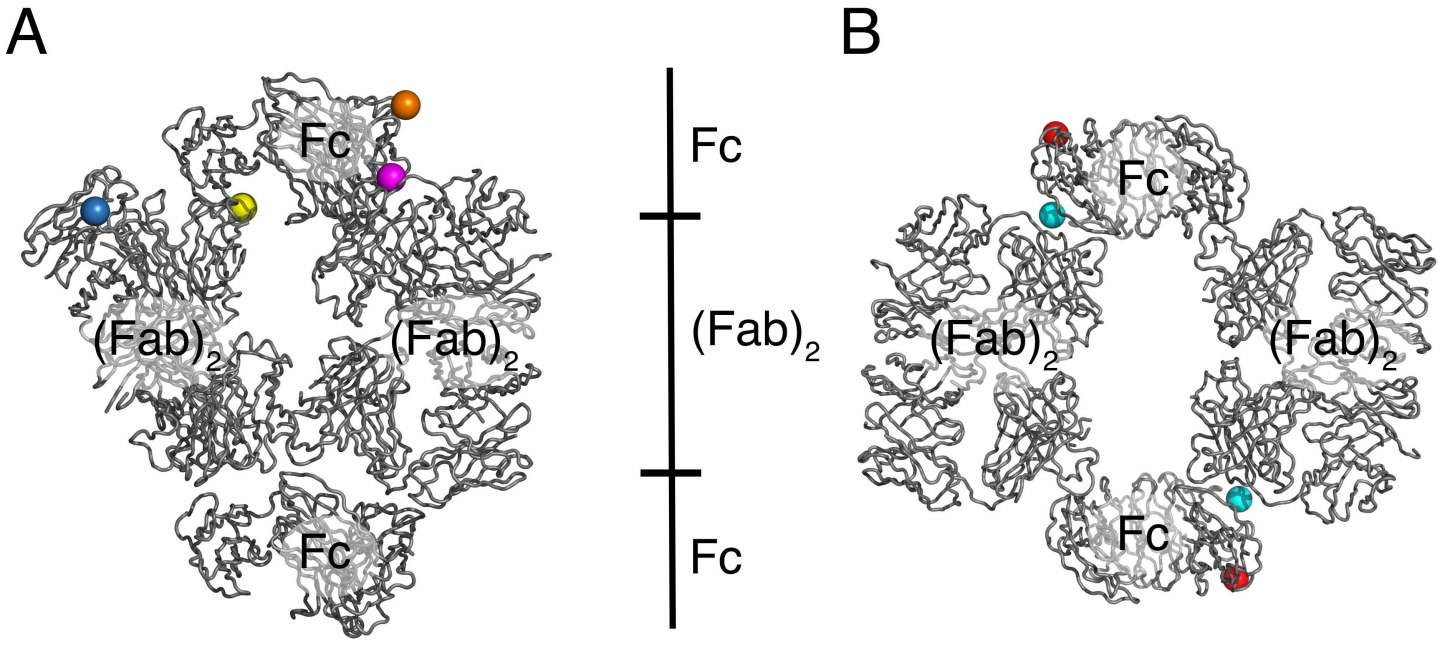

Figure S2, related to Figure 2

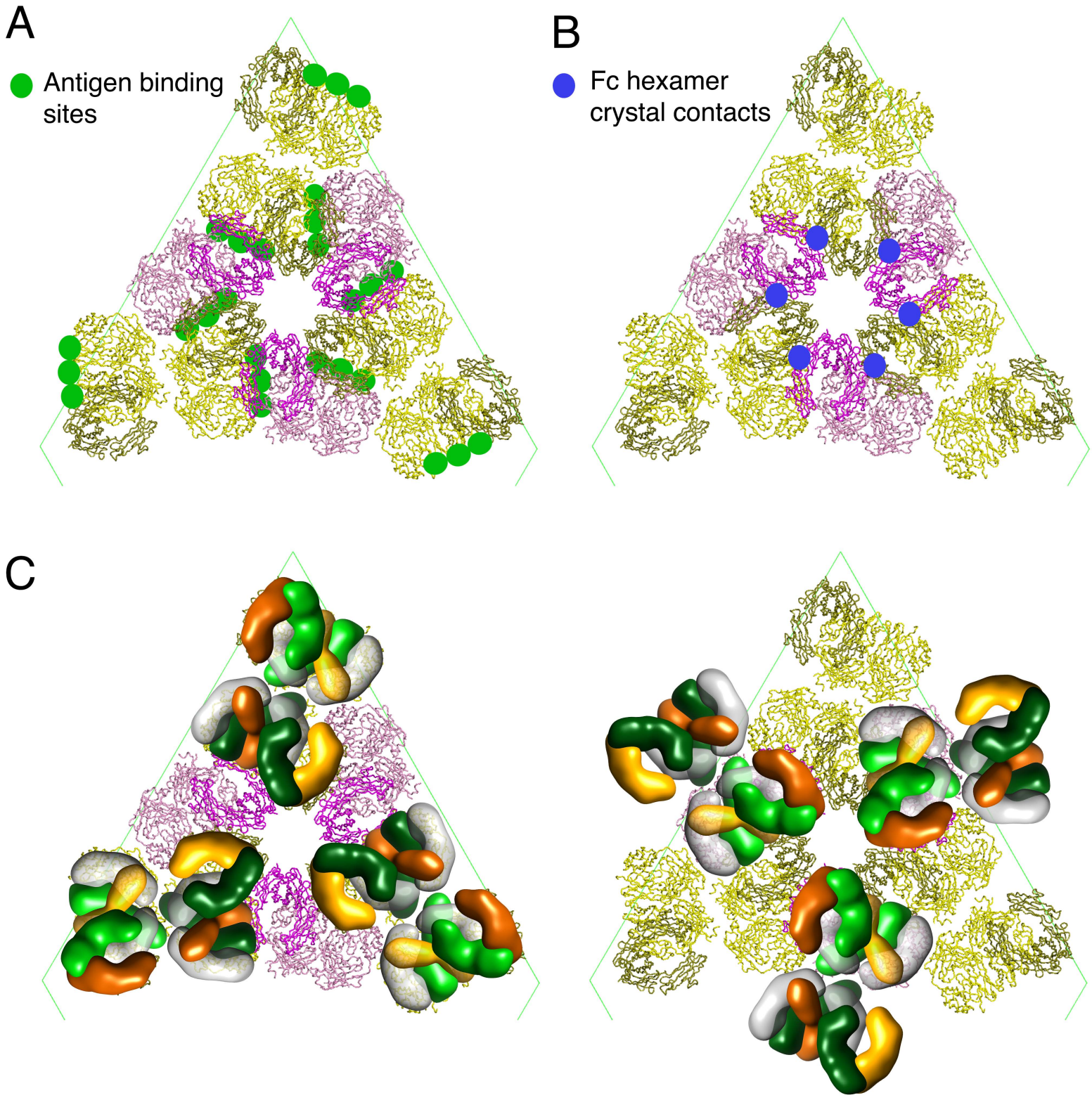

Figure S3, related to Figure 3

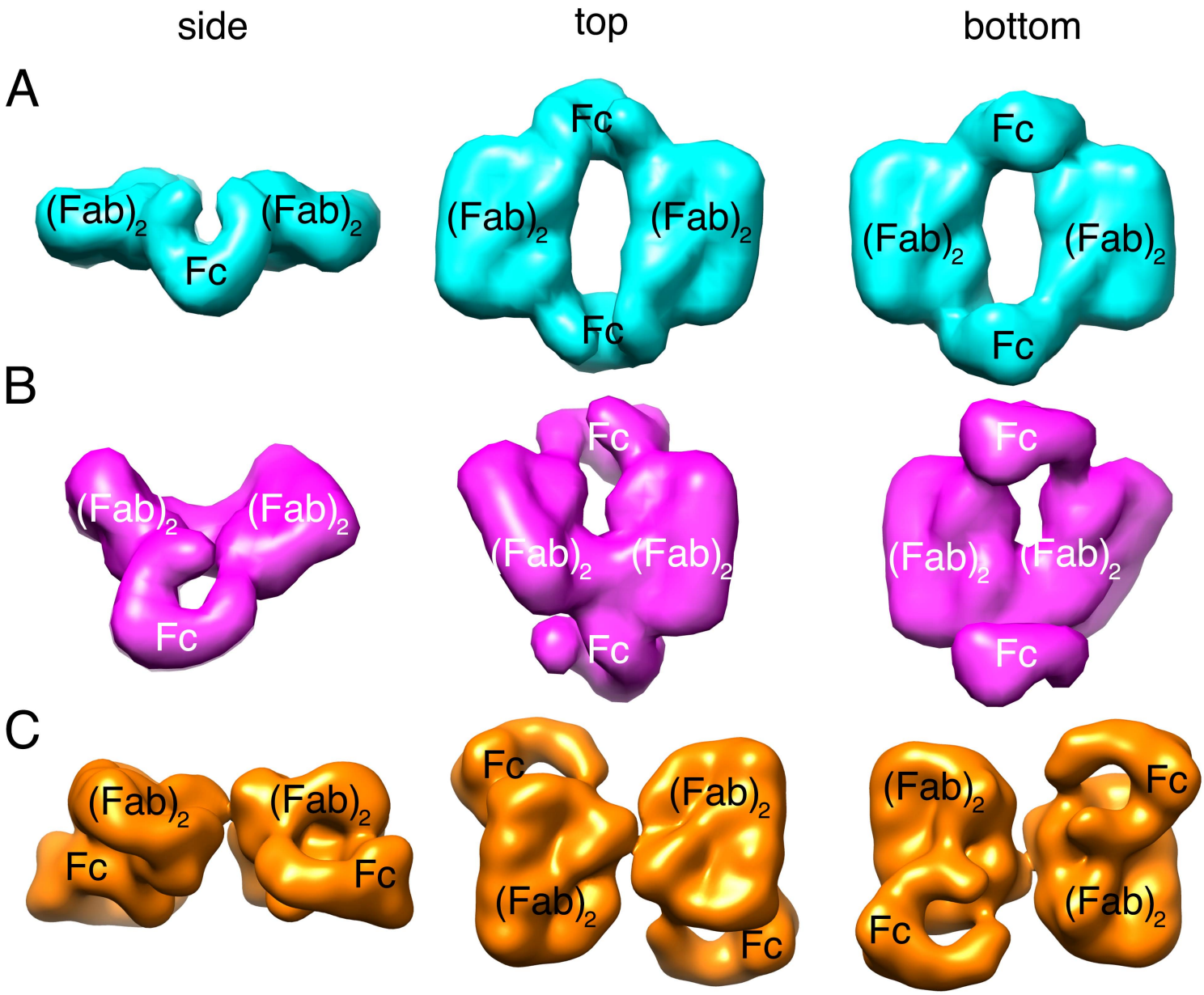

Figure S4, related to Figure 4

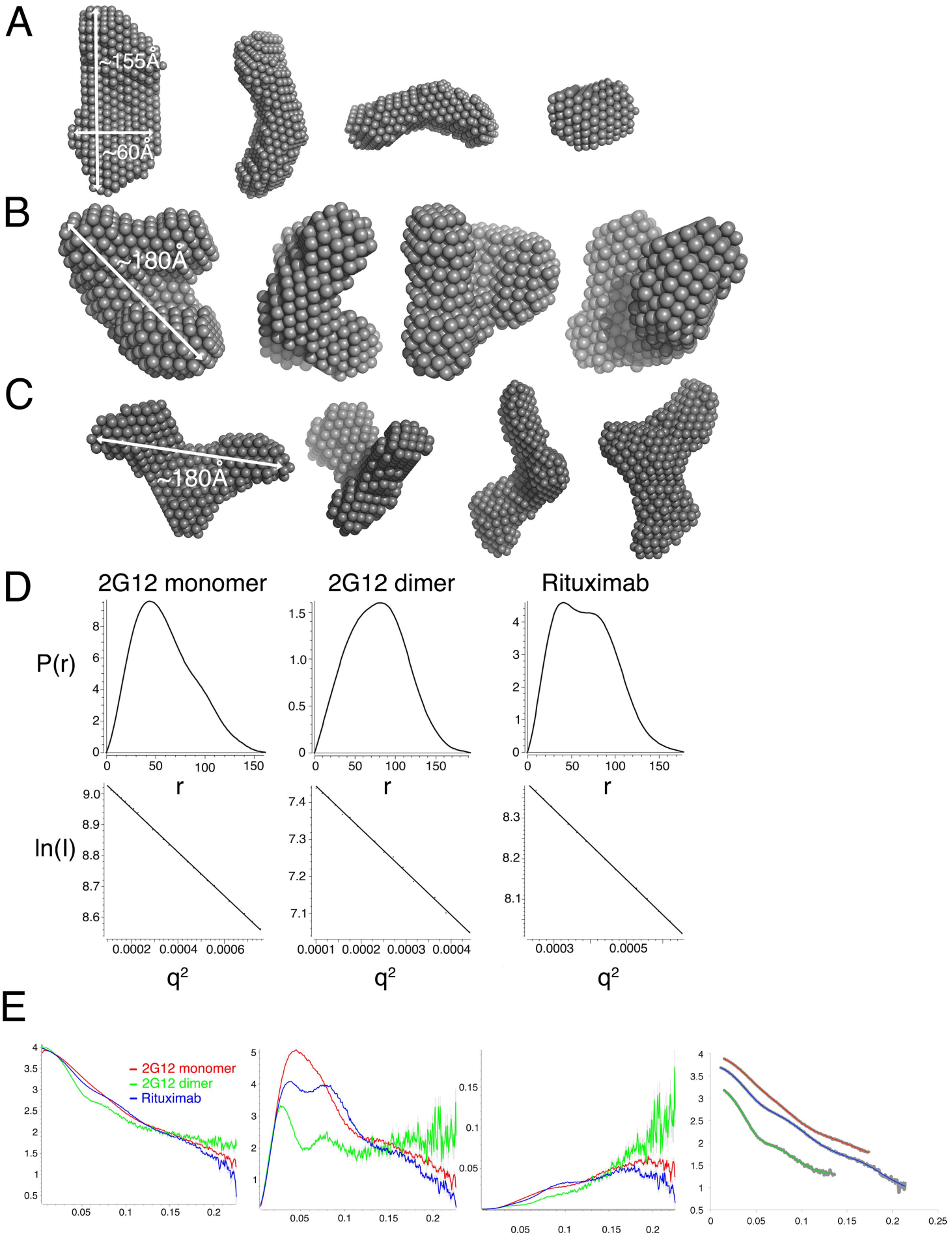

Figure S5, related to Figure 5

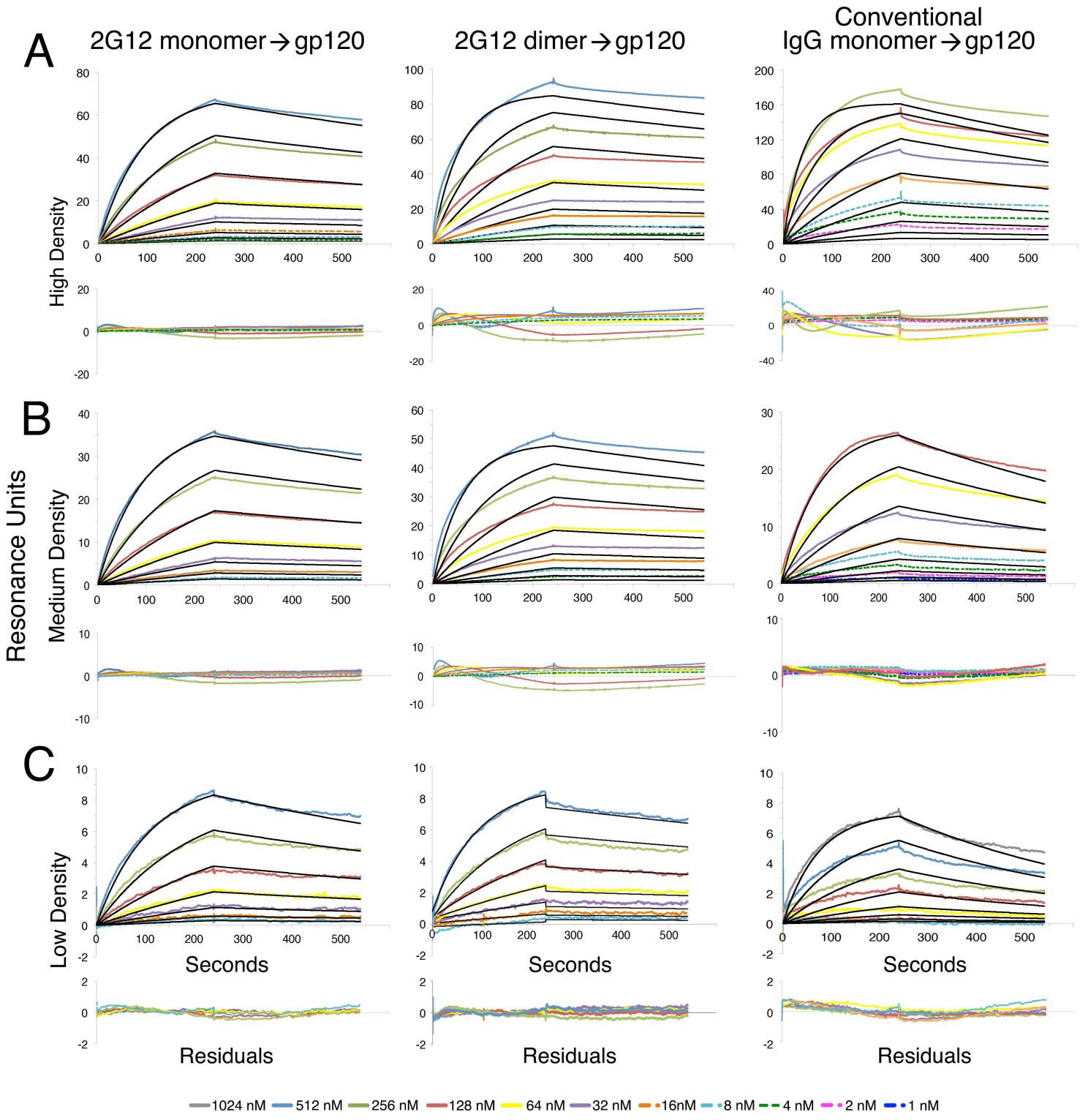

Figure S6, related to Figure 6